Nanoscale

COMMUNICATION

Check for updates

High bandwidth semipolar (20−21) micro-LED-based white light-emitting diodes utilizing perovskite quantum dots and organic emitters in color-conversion layers for visible light communication and solid-state lighting applications

Annada Sankar Sadhu,[a,b] Yi-Hua Pai,[a] Li-Yin Chen, [ID] *[a] Chung-An Hsieh,[a] Hao-Wu Lin [ID] [c] and Hao-Chung Kuo [ID] *[a,d]

We demonstrate semipolar (20−21) micro-LED-based high-bandwidth WLEDs utilizing perovskite QDs and organic emitters in color-conversion films. The WLEDs exhibit a bandwidth in excess of 1 GHz and a CCT of 6141 K, making these devices suitable for visible light communication and lighting applications.

Introduction

Wireless communication technology has had a major impact on our lives in recent decades. Most wireless communication currently relies on radio frequency and microwaves, but the spectrum is becoming increasingly crowded due to the rapid growth of mobile data and Internet of Things applications. One solution to this problem is visible light communication (VLC), which uses a very wide frequency band ranging from 400 THz to 800 THz (400 nm to 800 nm in wavelength). The widespread use of solid-state lighting sources, such as white light-emitting diodes (WLEDs), can be modulated at high speeds to provide a data channel for VLC, enabling highly secure and energy-efficient data transmission.[1]

Commercially available WLEDs used for illumination are typically made by combining a blue LED chip with yellow phosphors.[2] However, the bandwidth of these conventional WLEDs is often limited by the long photoluminescence (PL) lifetimes of the phosphors and the resistive–capacitive (RC) delay of the blue LEDs, which can hinder high-speed VLC.[3] To

address this issue, micro-LEDs (µLEDs) are emerging as the most promising candidates for VLC implementation due to their small size, high efficiency, and low resistive–capacitive delay.[4,5] Lan *et al.* demonstrated a GaN-based blue µLED in different configurations of an array that provides a bandwidth of ~600 MHz and a data rate of 1 Gbps using the non-return-to-zero on–off keying (NRZ-OOK) format.[6] Subsequently, Wei *et al.* reported a single-pixel µLED exhibiting a bandwidth of 1 GHz and a data rate of 8.7 Gbps using the quadrature phase shift keying-orthogonal frequency division multiplexing (QPSK-OFDM) scheme.[7] Despite their excellent VLC capacity, the emission spectra of µLED chips are currently limited to the ultraviolet to green light range, due to the poor yield and efficiency in the case of red emission.[8,9] This limits their direct implementation as broadband white light sources for VLC. This limitation can be overcome by using color-converting materials such as quantum dots (QDs) and organic emitters with short photoluminescence (PL) lifetimes. QDs have several advantages, including wide absorbance, tunable emission wavelength, high photoluminescence quantum yield (PLQY), short PL lifetime, and cost-effective production,[10–14] and have been considered as promising color-converting materials, especially in display applications. Similarly, organic emitters are also potentially useful as color-converting materials due to their broad absorbance spectrum, wide visible light emission, large stock shift, high PLQY, and fast PL lifetime.[15,16] The use of a blue µLED and CdSe/ZnS quantum dots (QDs) to create a white light emitting diode (WLED) with a bandwidth of 0.63 GHz and a correlated color temperature (CCT) of ~20 000 K was demonstrated by Cao *et al.*[17] Ma *et al.* proposed the use of CsPb(Br/I)$_3$ perovskite quantum dots (PQDs) in µLED-based WLEDs, which resulted in a white-light bandwidth of 0.75 GHz with a tunable CCT.[18] Similarly, a commercial organic yellow emitter (Super Yellow) combined with a µLED (bandwidth of 60 MHz) was shown to produce a white light bandwidth of

[a]*Department of Photonics, Institute of Electro-Optical Engineering, College of Electrical and Computer Engineering, National Yang Ming Chiao Tung University, Hsinchu 30010, Taiwan. E-mail: lychen@nycu.edu.tw, hckuo@faculty.nctu.edu.tw*
[b]*International Ph.D. Program in Photonics (UST), College of Electrical and Computer Engineering, National Yang Ming Chiao Tung University, Hsinchu 30010, Taiwan*
[c]*Department of Materials Science and Engineering, National Tsing Hua University, Hsinchu 30013, Taiwan*
[d]*Semiconductor Research Center, Hon Hai Research Institute, Taipei 11492, Taiwan*

0.53 MHz and a data rate of 1.68 Gbps using DC-biased optical OFDM.[19] One strategy to further increase the bandwidth of a visible light communication (VLC) system is to use semipolar plane (20–21) grown μLEDs as pumping sources. These μLEDs have a lower quantum-confined Stark effect (QCSE) and a higher overlap between electron and hole wave functions compared to *c*-plane LEDs, leading to a fast photoluminescence (PL) lifetime, high bandwidth, high luminous efficiency, and minimal shift in the emission spectra. These characteristics make semipolar plane (20–21) grown μLEDs suitable for use in VLC and lighting applications.[9,20]

In this work, we propose a high-bandwidth white light system that combines a single-pixel semipolar (20–21) blue μLED, a phenothiazine/dimesitylborane-based organic blue emitter (CC-MP3), green-emitting $CH_3NH_3PbBr_3$ perovskite quantum dots (PQDs), and a commercially available red-emitting phosphorescent emitter bis(2-(9,9-diethyl-fluoren-2-yl)-1-phenyl-1*H*-benzo[*d*] imidazolato)(actylacetonate)iridium(III) (Ir(fbi)$_2$(acac)). This combination has not been previously studied for its optical and frequency response performance in both VLC and lighting applications. By designing the color-conversion layers appropriately, the white light emitting diodes (WLEDs) achieved a bandwidth of approximately 1.0 GHz, a CCT ranging from 4000 K to 6000 K, and a color rendering index (CRI) ranging from 61.3 to 82.4. To the best of our knowledge, this bandwidth is the highest among recently reported μLED-based VLC systems. The high bandwidth is attributed to the high modulation bandwidth of the μLED and the fast PL response of the emitters, which reduce the attenuation of high-frequency signals. We believe that the high bandwidth and excellent illuminating characteristics of the proposed WLED system will be highly beneficial for both VLC and lighting applications in practical settings.

Experimental section

Materials

10,10′-((10-Mesityl-10*H*-phenothiazine-3,7-diyl)bis(3,1-pheny-lene)) bis-(10*H*-phenothiazine) (CC-MP3) and $CH_3NH_3PbBr_3$ PQDs (with an average size of 14 nm) were synthesized according to our previous works.[21,22] Ir(fbi)$_2$(acac) was purchased from Lumtec (New Taipei City, Taiwan) and poly(methyl methacrylate) (PMMA) powder was purchased from Sigma-Aldrich (St Louis, MO, USA). The molecular structures of CC-MP3 and Ir(fbi)$_2$(acac) are shown in Fig. 1.

Fabrication of color-conversion films

To obtain a uniform solution, 15 mg of CC-MP3 and 2 mg of Ir (fbi)$_2$(acac) were individually dissolved in 1 mL of toluene. 120 mg of PMMA powder was mixed with 1 mL of toluene and stirred for 24 hours at 50 °C to produce a transparent glue-like solution. The color-conversion films, B1, B2, and B3, were fabricated by dispersing color-conversion materials with different concentrations in PMMA, which is a common matrix due to its optical transparency, moderate rigidity and stability, and
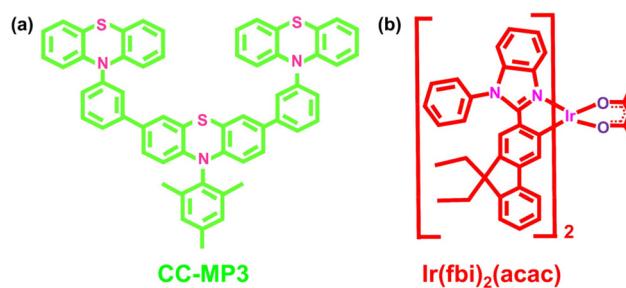

Fig. 1 Molecular structures of (a) CC-MP3 and (b) Ir(fbi)$_2$(acac).

good processability. B1 was prepared by doping 13.8 wt% $CH_3NH_3PbBr_3$ and 0.56 wt% Ir(fbi)$_2$(acac) into PMMA. B2 was prepared by doping 4.2 wt% CC-MP3, 17.4 wt% $CH_3NH_3PbBr_3$, and 0.56 wt% Ir(fbi)$_2$(acac) into PMMA, while B3 was prepared by only doping 4.2 wt% CC-MP3 and 0.56 wt% Ir(fbi)$_2$(acac) into PMMA. These are the optimized concentrations to obtain the CCT of white light on the Planckian locus. To further understand the bandwidth performance of each color conversion material, CC-MP3, $CH_3NH_3PbBr_3$, and Ir(fbi)$_2$(acac) were also doped into PMMA separately in weight ratios of 4.2%, 17.4%, and 1.67%, respectively. All the color-conversion films were drop-cast onto quartz substrates and dried in a N_2-filled glovebox overnight, resulting in solvent-free uniform films.

Instrumentation

The absorption spectra, PL emission spectra, and PLQYs of the color-conversion films were recorded using a FLUOROMAX-PLUS-C spectrofluorometer (Horiba, NJ, USA). The PL emission spectra and PLQYs were obtained by exciting the samples at 405 nm, and an integrating sphere was used for PLQY measurements. Time-resolved photoluminescence (TRPL) was recorded using a time-correlated single photon counting module (SPC-130-EM, Becker & Hickl GmbH) under excitation with a 375 nm laser diode (LDH-P-C-375M, PicoQuant). The optical properties of the WLED systems, including the luminescence spectra, CCT, CIE color coordinates, and CRI, were determined using a spectrometer (QE65000, Ocean Optics) equipped with an integrating sphere (Isuzu Optics Corp., Hsinchu, Taiwan).

Fabrication of the semipolar blue μLED

Fig. 2 shows the schematic of the semipolar (20–21) μLED. The device architecture and fabrication steps were similar to those in previous works.[9,23] A sapphire substrate patterned by reactive ion etching (RIE) was used to grow semipolar (20–21)-oriented GaN layers *via* metal organic chemical vapor deposition (MOCVD). Ge-doped GaN was employed at the beginning of the epitaxy process to prevent stacking faults. Then, an 8 μm-thick bulk un-doped GaN layer was deposited on top of the Ge-doped GaN layer. An n-GaN layer (1.5 μm) served as the active layer, followed by an InGaN (3 nm)/GaN (5 nm) single quantum well (SQW) and a 100 nm-thick p-type GaN layer. Subsequently, a p-type metal contact was fabricated by deposit-
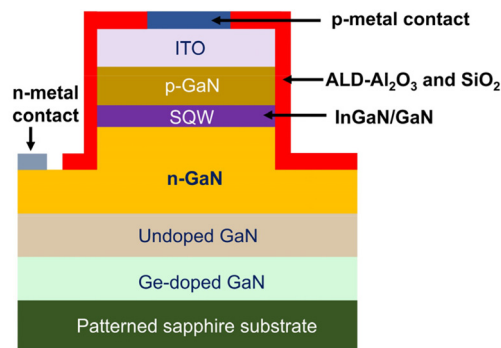
Fig. 2 Schematic structure of the semipolar (20−21) μLED.

ing an ITO (225 nm) layer onto the p-type GaN layer, which was followed by mesa etching using HCl and inductively coupled plasma reactive ion etching (ICP-RIE) to create a mesa depth. Thermal annealing was then performed to improve the current-spreading layer and form ohmic contact for the p-type metal contact. The electrode was deposited in the configuration of Ti (20 nm)/Al (125 nm)/Ni (45 nm)/Au (75 nm) using electron beam evaporation. To prevent leakage current caused by sidewall defects, Al_2O_3 (30 nm) and SiO_2 (200 nm) were fabricated using atomic layer deposition (ALD) and plasma-enhanced chemical vapor deposition (PECVD), respectively, as passivation layers. Finally, Ti (20 nm)/Al (250 nm)/Au (300 nm) was deposited to create sidewall reflectors and a metal pad. The chip diameter of the μLED was 100 μm.

Bandwidth measurement setup

Fig. 3 shows the schematic structure of the bandwidth measurement system for blue μLED and white light systems. In each case, a bias tee was used to run the μLED by combining an AC current from a vector network analyzer with a DC current bias (HP 8720ES). The blue light from the μLED was captured through an optical fiber that was attached to a photodetector (SPA-3, Graviton). The optical signal (blue light) was
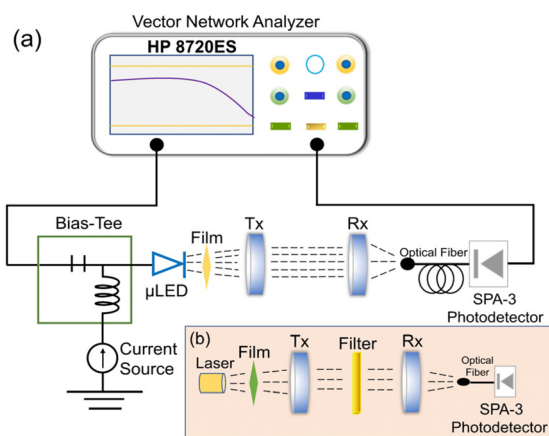
converted to an electrical signal by the photodetector and then sent to a vector network analyzer (VNA) for frequency response analysis. By placing the color-conversion films in front of the μLED and collimating the resulting white light through Tx and Rx lenses (without filters), the white light was then captured and sent *via* an optical fiber to the photodetector. The frequency responses of CC-MP3, $CH_3NH_3PbBr_3$, and $Ir(fbi)_2(acac)$ color-conversion films were measured by using a blue laser (PL 450B, OSRAM) instead of the μLED (Fig. 3b). In this stage, a 475 nm long-pass optical filter (5CGA-475, Newport) was used to block the remnants of blue light from the laser, so that the collected optical signal was only from CC-MP3, $CH_3NH_3PbBr_3$, and $Ir(fbi)_2(acac)$.

Results and discussion

The electro-optical characteristics of the semipolar μLED are shown in Fig. 4. At a maximum current density of 2500 A cm^{-2}, the applied current was 196 mA (Fig. 4a). The turn-on voltage of the semipolar μLED was 3 V at a current density of 39.9 A cm^{-2}, which is similar to that of *c*-plane devices. Additionally, an output power of 28.9 mW at 196 mA suggests that the μLED is suitable for pumping color-conversion films in visible light communication (VLC) and lighting applications. In Fig. 4(b), the electroluminescence (EL) spectra of the semipolar blue μLED are shown at various driving currents. At a driving current of 196 mA, a peak wavelength of 443 nm and a full width half maximum (FWHM) of 24.9 nm were obtained. The small FWHM indicates a high-quality epitaxial structure. The dependence of the peak wavelength and FWHM on the applied current is shown in Fig. 4(c). A slight blue shift of 3.28 nm in the peak wavelength was observed when the applied current was increased from 7 mA to 196 mA, but it stabilized after 60 mA (765 A cm^{-2} in current density). This minor blue shift may be due to the reduction of the polar-
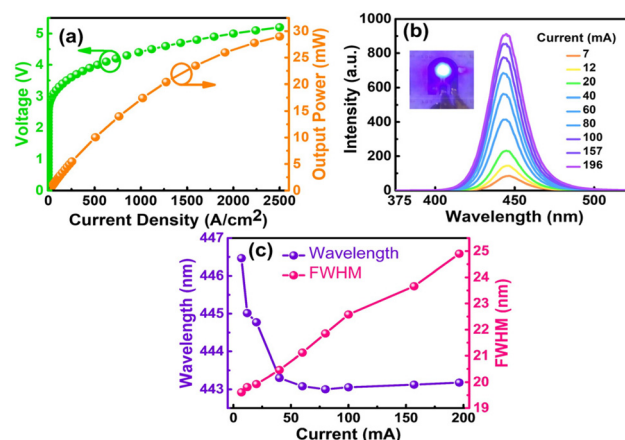

Fig. 3 Bandwidth measurement system architecture for (a) a white light system and (b) color-conversion films.

Fig. 4 (a) $P–J–V$ characteristics of the μLED. (b) EL spectra at various applied currents; the inset shows an optical image of the device under bias with a mesa diameter of 100 μm. (c) Change in the peak wavelength and FWHM of the device under applied currents.

ization-related electric field in the single quantum well grown on semipolar facets, which reduces the quantum confined Stark effect (QCSE). The FWHM also increased slightly from 19.6 to 24.9 nm (5.3 nm) when the driving current increased from 7 mA to 196 mA. This increase in FWHM is likely caused by the band filling effect in the InGaN/GaN single quantum well, which can be minimized by optimizing the chip fabrication process of the μLEDs.

The details of materials analysis, including transmission electron microscopy (TEM) of PQDs and nuclear magnetic resonance (NMR) spectroscopy and high-resolution mass spectrometry (HRMS) results of CC-MP3, have been previously reported in our studies.[21,22] The UV-visible absorbance and PL emission spectra of CC-MP3, PQDs, and Ir(fbi)$_2$(acac) are shown in Fig. 5. The wide absorption spectra with an absorption onset at 466 nm, 530 nm, and 525 nm for CC-MP3, PQDs, and Ir(fbi)$_2$(acac), respectively, indicate that the blue μLED can efficiently excite all the color-conversion materials. The wide PL emission of CC-MP3 has an emission peak at 477 nm, a shoulder at 504 nm, and a FWHM of 66 nm. The PQDs showed a narrow emission spectrum with a peak of 527 nm (FWHM of 28 nm). The commercial emitter Ir(fbi)$_2$(acac) also exhibits wide PL emission with two peaks at 568 nm and 618 nm, and a shoulder at 685 nm (FWHM of ~115 nm). The PLQY of CC-MP3 and PQDs in the solid-state thin films was 63% and 100%, respectively, indicating that they are very promising materials for color conversion.

To further understand the photophysical properties of the color-conversion materials, we first measured their PL lifetimes. Fig. 6a and b show that the PL lifetimes (to 1/e of the initial value) of CC-MP3, CH$_3$NH$_3$PbBr$_3$, and Ir(fbi)$_2$(acac) are 3.96 ns, 10 ns, and 15 ns, respectively, based on their central emission of 477, 528, and 568 nm. These lifetimes are much faster than those of conventional phosphors and comparable to those of recently reported materials for VLC and solid-state lighting.[24–26] The modulation bandwidths of CC-MP3, CH$_3$NH$_3$PbBr$_3$, and Ir(fbi)$_2$(acac) were 170 MHz, 325 MHz, and 110 MHz, respectively, which suggest much higher communication speeds and channel capacities for VLC compared to conventional phosphors and CdSe/ZnS QDs used in WLED systems. These materials typically only have bandwidths of
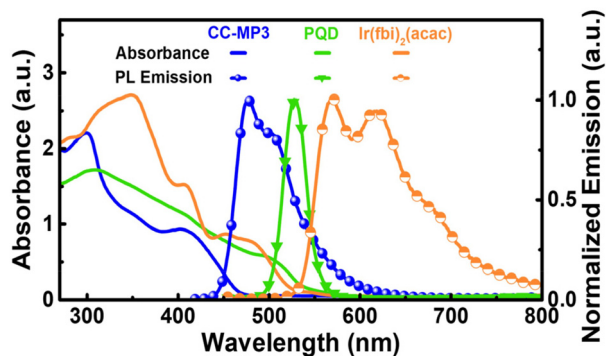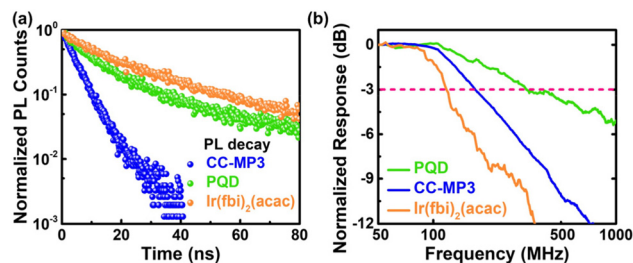
Fig. 6 (a) PL decay curve of neat CC-MP3, neat PQDs, and neat Ir(fbi)$_2$(acac) films. (b) −3 dB bandwidth of emitters.

several to tens of MHz.[17,27] Previous research has shown that there is a relationship between the cut-off frequency ($f_{3\,dB}$) and the PL lifetime (τ_{PL}) of CdSe/ZnS QDs using the equation $f_{3\,dB} = \sqrt{3}/2\pi\tau_{PL}$.[28] However, a negative correlation between $f_{3\,dB}$ and τ_{PL} has been observed by many researchers, indicating that this equation does not always provide accurate quantitative results for materials like PQDs, organic emitters and aggregation-induced emission (AIE) materials.[24,26,29,30] In our study, we also observed that the modulation bandwidth of the color-conversion materials did not show the negative correlation seen in CdSe/ZnS QDs. It is worth noting that the concentrations of CC-MP3, PQDs, and Ir(fbi)2(acac) in the PMMA matrix vary significantly in the color-conversion layers. However, previous studies have demonstrated that the −3 dB bandwidth of a composite film remains relatively constant with changes in the emitter concentration.[15] As a result, the −3 dB bandwidth of the emitters depicted in Fig. 6 can serve as an indicator of the modulation capability of the color-conversion layers.

Three white LED (WLED) systems, S1, S2, and S3, were created by overlaying the color-conversion films, B1, B2, and B3, respectively, on the μLED. The emission spectra and the color performance of the resulting WLED systems are shown in Fig. 6. As shown in Fig. 7a, S1 exhibits emission peaks at 443 nm and 530 nm, which are contributed by the μLED and PQDs, respectively. Similarly, the peaks at 568 nm, 602 nm and 670 nm are from Ir(fbi)$_2$(acac). It was also observed that PQDs enhance green emission in the WLED. However, the low intensity in the region around 500 nm in the emission spectrum reduced its color rendering capability. As a result, S1 provides white light with a CCT of 6141 K, a chromaticity coordinate of (0.3196, 0.3277) on the CIE 1931 color space, and a low CRI of R_a = 61.3. To improve the performance of WLED systems at around 500 nm in the wavelength region, we added CC-MP3 in the composite film, resulting in a new film called B2. The white light spectra of S2 (Fig. 7b) had a CCT of 5561 K, CIE coordinates at (0.3311, 0.3117), and a high CRI of 82.4, while S3 (Fig. 7c) exhibited a CCT of 4089 K, CIE coordinates at (0.3787, 0.3828), and a moderate CRI of ~72. The CCT and CRI of S3 are lower compared to those of S2 because S3 does not contain PQDs. However, the CRI of S3 is improved compared to that of S1 because it includes CC-MP3. The corresponding CIE coordinates of the three WLEDs are denoted in
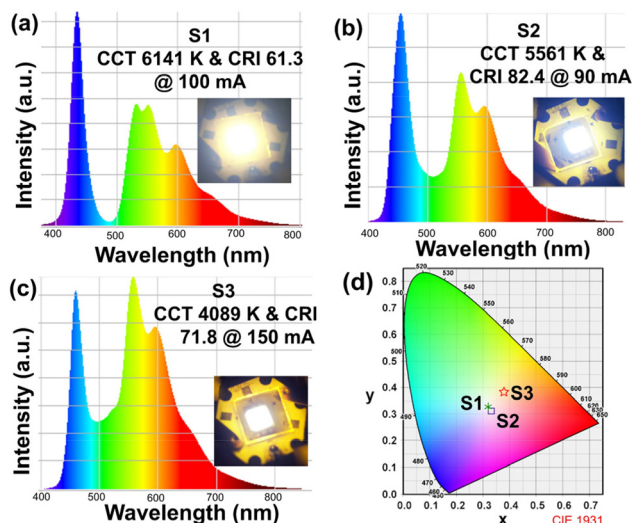
Fig. 5 Absorbance and PL emission spectra of emitters.

Fig. 7 White light emission spectra of (a) S1, (b) S2, and (c) S3. (d) CIE coordinates of the S1, S2, and S3 WLED systems.

Fig. 9 Stability of CC-MP3 and PQDs after 180 days (a) in the optical and (b) in the frequency response performance.

Fig. 7d. The three different applied currents shown in Fig. 7 were chosen to achieve the highest attainable CRI in each case. However, varying the applied current did not result in significant changes in the CCT and CRI. For instance, when an applied current of 196 mA was used, S1, S2, and S3 showed CCTs of 6016 K, 5760 K, and 4203 K, respectively, and CRIs of 60.7, 80.8, and 69.4, respectively, indicating excellent color stability. Therefore, these white light emitters are suitable for a variety of applications, such as traffic communication, indoor lighting, and vehicle headlights. The color performance of these devices can be further enhanced by optimizing and improving the fabrication of μLED devices and developing new color-conversion emitters with wide emission spectra in the future.

The −3 dB bandwidth of a VLC-LED depends on the radiative carrier lifetime (τ_r), the non-radiative carrier lifetime (τ_{nr}), and the RC constant.[28] However, the −3 dB BW of a device with an active region area of 100 μm or less is confined by its τ_r.[31] As shown in Fig. 8a, increasing the injected current density of the μLED reduces its τ_r, resulting in an increase in

its bandwidth, which can be attributed to the internal electric field screening and fast carrier lifetime at higher currents in the active region.[9] As a result, the semi-polar μLED at a driving current of 196 mA showed a −3 dB bandwidth of 1230 MHz. Additionally, an increase in the BW with the injected current density (inset of Fig. 8a) indicates that the bandwidth is dependent on the carrier recombination lifetime rather than being constrained by the RC delay. The bandwidths of S1, S2, and S3 (Fig. 8b) were 1008, 952, and 988 MHz, respectively, at an applied current density of 2.5 kA cm^{-2}. These values are among the highest reported in the literature for VLC using μLEDs and demonstrate a superior communication channel capacity for VLC.[17,18,24,26] However, a reduction in white-light bandwidths was observed compared to the blue μLED due to the presence of high-frequency noise when the blue light passed through the composite films at high applied currents. These noises reduced the gain in BW exhibited by the μLED at higher current. In particular, the addition of an extra optical component (CC-MP3) in S2 led to an increase in noise levels,[26] which further reduced the white-light bandwidth compared to S1 and S3. Nonetheless, the white-light bandwidths were still higher due to the larger bandwidth and optical power of the μLEDs.

Organic emitters and PQDs are generally prone to instability when exposed to atmospheric conditions.[32–34] Therefore, the stability of CC-MP3 and PQD color-conversion films was evaluated after 180 days of storage (Fig. 9) in a humidity control cabinet. Both samples showed minor degradation of approximately 9% in the PL intensity and 11% in the bandwidth for CC-MP3, and 14% in the PL intensity and 15% in the bandwidth for PQDs. These values are lower than those reported in previous studies.[24,26] The PQDs also exhibited a 4 nm blue shift which may due to the phase segregation of a halide component, which is still acceptable in SSL and VLC.
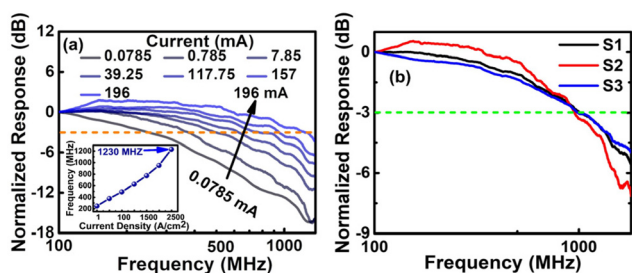

Fig. 8 (a) Variation in the bandwidths of the μLED under different driving currents and equivalent applied current densities (inset). (b) White light bandwidths at 196 mA.
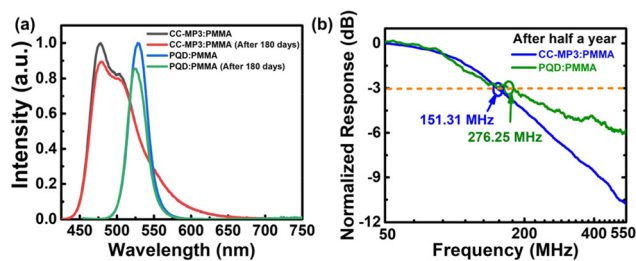
Conclusions

In this work, we have presented three high-bandwidth WLED systems that combine a semipolar blue μLED with color-conversion layers utilizing organic emitters, CC-MP3 and Ir (fbi)$_2$(acac), and CH$_3$NH$_3$PbBr$_3$ perovskite quantum dots. The

CC-MP3 and PQDs exhibited a modulation bandwidth of 170 MHz and 325 MHz, respectively, due to their fast PL lifetimes of 3.96 ns and 10 ns. The three WLED systems produced high-quality white light with correlated color temperatures (CCTs) of 6141 K, 5561 K, and 4089 K and color rendering indices (CRIs) of 61.3, 82.4, and ~72, respectively. In addition, they provided high-bandwidth white light with bandwidths of 1008, 952, and 988 MHz, respectively, which are among the highest reported in the literature. CC-MP3 and $CH_3NH_3PbBr_3$ also demonstrated significant stability after 180 days of storage. These results offer a promising solution for high-performance visible-light sources for fast, secure, and energy-efficient wireless transmission.

Author contributions

Conceptualization, visualization, and writing – original draft preparation: A.S.S. and L.Y.C.; methodology: A.S.S., Y.H.P, L.Y.C. and H.C.K.; software: L.Y.C. and H.C.K.; resources: L.Y.C., H.W.L. and H.C.K.; data curation: A.S.S., Y.H.P. and C. A.H.; writing – review and editing: L.Y.C., H.W.L. and H.C.K.; supervision: L.Y.C. and H.C.K.; project administration: L.Y.C. and H.C.K.; funding asset: L.Y.C. and H.C.K. All authors have read and approved the published version of the manuscript.

Conflicts of interest

There are no conflicts to declare.

Acknowledgements

References

1 A. Jovicic, J. Li and T. Richardson, *IEEE Commun. Mag.*, 2013, **51**, 26–32.

2 C. Yang, X. Liang, X. Di, P. Li, G. Hu, R. Cao and W. Xiang, *Ceram. Int.*, 2016, **42**, 14526–14532.

3 R. Wan, L. Wang, J. Huang, X. Yi, H. C. Kuo and J. Li, *Adv. Photonics Res.*, 2021, **2**, 2100093.

4 L. Yu, L. Wang, Z. Hao, Y. Luo, C. Sun, B. Xiong, Y. Han, J. Wang and H. Li, *Semicond. Sci. Technol.*, 2021, **37**, 023001.

5 T. Y. Lee, L. Y. Chen, Y. Y. Lo, S. S. Swayamprabha, A. Kumar, Y. M. Huang, S. C. Chen, H. W. Zan, F. C. Chen, R. H. Horng and H. C. Kuo, *ACS Photonics*, 2022, **9**, 2905–2930.

6 H. Y. Lan, I. C. Tseng, Y. H. Lin, G. R. Lin, D. W. Huang and C. H. Wu, *Opt. Lett.*, 2020, **45**, 2203–2206.

7 Z. Wei, Z. Liu, X. Liu, L. Wang, L. Wang, C. Yu and H. Y. Fu, *Opt. Lett.*, 2021, **46**, 4670–4673.

8 X. He, E. Xie, M. S. Islim, A. A. Purwita, J. J. McKendry, E. Gu, H. Haas and M. D. Dawson, *Photonics Res.*, 2019, **7**, B41–B47.

9 S. W. H. Chen, Y. M. Huang, Y. H. Chang, Y. Lin, F. J. Liou, Y. C. Hsu, J. Song, J. Choi, C. W. Chow, C. C. Lin and R. H. Horng, *ACS Photonics*, 2020, **7**, 2228–2235.

10 K. J. Singh, X. Fan, A. S. Sadhu, C. H. Lin, F. J. Liou, T. Wu, Y. J. Lu, J. H. He, Z. Chen, T. Wu and H. C. Kuo, *Photonics Res.*, 2021, **9**, 2341–2350.

11 K. J. Singh, T. Ahmed, P. Gautam, A. S. Sadhu, D. H. Lien, S. C. Chen, Y. L. Chueh and H. C. Kuo, *Nanomaterials*, 2021, **11**, 1549.

12 C. Sun, Z. Gao, H. Liu, L. Wang, Y. Deng, P. Li, H. Li, Z. H. Zhang, C. Fan and W. Bi, *Chem. Mater.*, 2019, **31**, 5116–5123.

13 Z. Gao, X. Wang, Y. Bai, C. Sun, H. Liu, L. Wang, S. Su, K. Tian, Z. H. Zhang and W. Bi, *Appl. Phys. Lett.*, 2019, **115**, 153103.

14 S. Su, J. Tao, C. Sun, D. Xu, H. Zhang, T. Wei, Z. H. Zhang, Z. Wang, C. Fan and W. Bi, *Chem. Eng. J.*, 2021, **419**, 129612.

15 M. T. Sajjad, P. P. Manousiadis, H. Chun, D. A. Vithanage, S. Rajbhandari, A. L. Kanibolotsky, G. Faulkner, D. O'Brien, P. J. Skabara, I. D. Samuel and G. A. Turnbull, *ACS Photonics*, 2015, **2**, 194–199.

16 C. Y. Su, Y. C. Wu, C. H. Cheng, W. C. Wang, H. Y. Wang, L. Y. Chen, H. C. Kuo and G. R. Lin, *ACS Appl. Electron. Mater.*, 2020, **2**, 3017–3027.

17 H. Cao, S. Lin, Z. Ma, X. Li, J. Li and L. Zhao, *IEEE Electron Device Lett.*, 2018, **40**, 267–270.

18 Z. Ma, X. Li, C. Zhang, L. Turyanska, S. Lin, X. Xi, J. Li, T. Hu, J. Wang, A. Patanè and L. Zhao, *ACS Appl. Nano Mater.*, 2021, **4**, 8383–8389.

19 H. Chun, P. Manousiadis, S. Rajbhandari, D. A. Vithanage, G. Faulkner, D. Tsonev, J. J. D. McKendry, S. Videv, E. Xie, E. Gu and M. D. Dawson, *IEEE Photonics Technol. Lett.*, 2014, **26**, 2035–2038.

20 H. Zhang, P. Li, H. Li, J. Song, S. Nakamura and S. P. DenBaars, *Appl. Phys. Lett.*, 2020, **117**, 181105.

21 Y. J. Cheng, S. Y. Yu, S. C. Lin, J. T. Lin, L. Y. Chen, D. S. Hsiu, Y. S. Wen, M. M. Lee and S. S. Sun, *J. Mater. Chem. C*, 2016, **4**, 9499–9508.

22 S. W. Dai, B. W. Hsu, C. Y. Chen, C. A. Lee, H. Y. Liu, H. F. Wang, Y. C. Huang, T. L. Wu, A. Manikandan, R. M. Ho, C. S. Tsao, C. H. Cheng, Y. L. Chueh and H. W. Lin, *Adv. Mater.*, 2018, **30**, 1705532.

23 T. Wu, Y. Lin, Y. M. Huang, M. Liu, K. J. Singh, W. Lin, T. Lu, X. Zheng, J. Zhou, H. C. Kuo and Z. Chen, *Photonics Res.*, 2021, **9**, 2132–2143.

24 S. Mei, X. Liu, W. Zhang, R. Liu, L. Zheng, R. Guo and P. Tian, *ACS Appl. Mater. Interfaces*, 2018, **10**, 5641–5648.

25 Z. Tian, P. Tian, X. Zhou, G. Zhou, S. Mei, W. Zhang, X. Zhang, D. Li, D. Zhou, R. Guo and S. Qu, *Nanoscale*, 2019, **11**, 3489–3494.

26 Z. Wang, Z. Wei, Y. Cai, L. Wang, M. Li, P. Liu, R. Xie, L. Wang, G. Wei and H. Y. Fu, *ACS Appl. Mater. Interfaces*, 2021, **13**, 54143–54151.

27 H. Li, X. Chen, B. Huang, D. Tang and H. Chen, *IEEE Photonics Technol. Lett.*, 2013, **26**, 119–122.

28 N. Laurand, B. Guilhabert, J. Mckendry, A. E. Kelly, B. Rae, D. Massoubre, Z. Gong, E. Gu, R. Henderson and M. D. Dawson, *Opt. Mater. Express*, 2012, **2**, 250–260.

29 D. A. Vithanage, A. L. Kanibolotsky, S. Rajbhandari, P. P. Manousiadis, M. T. Sajjad, H. Chun, G. E. Faulkner, D. C. O'Brien, P. J. Skabara, I. D. W. Samuel and G. A. Turnbull, *J. Mater. Chem. C*, 2017, **5**, 8916–8920.

30 Y. Zhang, M. Jiang, T. Han, X. Xiao, W. Chen, L. Wang, K. S. Wong, R. Wang, K. Wang, B. Z. Tang and K. Wu, *ACS Appl. Mater. Interfaces*, 2018, **10**, 34418–34426.

31 M. Haemmer, B. Roycroft, M. Akhter, D. V. Dinh, Z. Quan, J. Zhao, P. J. Parbrook and B. Corbett, *IEEE Photonics Technol. Lett.*, 2018, **30**, 439–442.

32 A. S. Sadhu, Y. M. Huang, L. Y. Chen, H. C. Kuo and C. C. Lin, *Nanomaterials*, 2022, **12**, 985.

33 S. Biring, A. S. Sadhu and M. Deb, *Sensors*, 2019, **19**, 5124.

34 C. Y. Liu, A. S. Sadhu, R. Karmakar, C. S. Chu, Y. N. Lin, S. H. Chang, G. K. Dalapati and S. Biring, *Biosensors*, 2022, **12**, 774.